Functional Impact of Polar and Acidic Substitutions in the Lactose Repressor Hydrophobic Monomer·Monomer Interface with a Buried Lysine[†]

Hongli Zhan,*[,‡,§] Zhifei Sun,[‡] and Kathleen Shive Matthews[‡,||]

Department of Biochemistry and Cell Biology, Rice University, Houston, Texas 77005, W. M. Keck Center for Interdisciplinary Bioscience Training, Rice University, Houston, Texas 77005, and Department of Biochemistry and Molecular Biology, MS 3030, 3901 Rainbow Boulevard, The University of Kansas Medical Center, Kansas City, Kansas 66160

Received July 18, 2008; Revised Manuscript Received November 2, 2008

ABSTRACT: Despite predicted energetic penalties, the charged K84 side chains of tetrameric lactose repressor protein (LacI) are found buried within the highly hydrophobic monomer·monomer interface that includes side chains of V94 and V96. Once inducer binding has occurred, these K84 side chains move to interact with the more solvent-exposed side chains of D88 and E100′. Previous studies demonstrated that hydrophobic substitutions for K84 increased protein stability and significantly impaired the allosteric response. These results indicated that enhanced hydrophobic interactions at the monomer·monomer interface remove the energetic driving force of the buried charges, decreasing the likelihood of a robust conformational change and stabilizing the structure. We hypothesized that creating a salt bridge network with the lysine side chains by including nearby negatively charged residues might result in a similar outcome. To that end, acidic residues, D and E, and their neutral amides, N and Q, were substituted for the valines at positions 94 and 96. These variants exhibited one or more of the following functional changes: weakened inducer binding, impaired allosteric response, and diminished protein stability. For V96D and V96E, ion pair formation with K84 appears optimal, and the loss of inducer response exceeds that of the hydrophobic K84A and -L variants. However, impacts on functional properties indicate that stabilizing the buried positive charge with polar or ion pair interactions is not functionally equivalent to structural stabilization via hydrophobic enhancement.

Hydrophobic and electrostatic interactions act in concert to determine functionality in proteins, but the burial of charged residues exacts an energy cost (*1*−*5*). Nonetheless, such an arrangement, with a charged residue embedded in a hydrophobic subunit interface, is observed in the lactose repressor protein (LacI) and appears to contribute a critical element to inducer responsivity (*6*−*8*). In this study, we explore the functional outcome of adding negatively charged side chains or their amide derivatives in proximity to a positively charged side chain that is buried in a hydrophobic environment.

Lactose repressor protein (LacI)[1] has been widely utilized as a model for protein folding, allosteric transition, and protein engineering (*9*−*13*). In vivo, LacI binding to operator DNA represses the transcription of genes encoding Lac*Z*, *Y*, and *A* in the absence of lactose (*9, 13*). When lactose is available, the inducer metabolite generated from lactose (allolactose) binds to LacI and elicits a conformational change that reduces LacI affinity for the operator site by >1000-fold, allowing transcription of the lactose metabolic genes. In this process, the subunit interface reorganizes, moving K84 and K84′ side chains from their buried, apolar environment in DNA-bound LacI to an environment with greater solvent exposure and positioned to form a side chain ion pair interaction in IPTG-bound LacI (*7, 14*). These distinct changes in structure reflect the different states within the LacI functional cycle.

LacI is a homotetramer, formed as a dimer of dimers (*7, 14, 15*). Within the tetramer, each dimer can bind operator DNA, and each monomer can bind inducer. The LacI monomer contains five regions, and inducer binds at the intersection of the N- and C-subdomains (*7, 14, 15*) (Figure 1A). In the DNA-bound structure of a LacI dimer, the side chains of K84 and K84′ (one from each monomer) are almost completely buried within the N-subdomain monomer·monomer interface and are stabilized by a presumed anion and hydrogen bonds with the backbone at V94 and V96′ (*7, 14*) (Figure 1B). This interface is otherwise composed of two hydrophobic β-strands that encompass V66, L71, V80, I83, V95, and I123 (*7, 14*). Not only is the K84 side chain charge buried in a hydrophobic environment, two like charges are close together. Once inducer binding has occurred (and also in the unliganded structure), the K84 side chains move out of the hydrophobic interface toward solvent and are stabilized by interacting with the charged side chains of D88 and E100 (Figure 1B). Thus, K84 has the properties of a toggle

[†] This work was supported by NIH Grant GM22441 and Robert A. Welch Foundation Grant C-576 to K.S.M.

* To whom correspondence should be addressed. Telephone: (713) 348-4936. Fax: (713) 348-6149. E-mail: zhanhl@rice.edu.

[‡] Department of Biochemistry and Cell Biology, Rice University.

[§] The University of Kansas Medical Center.

[||] W. M. Keck Center for Interdisciplinary Bioscience Training, Rice University.

[1] Abbreviations: LacI, lactose repressor protein; IPTG, isopropyl β-D-thiogalactoside; ONPF, *o*-nitrophenyl β-D-fucopyranoside; TMD, targeted molecular dynamics.

10.1021/bi801357f CCC: $40.75
Published on Web 01/23/2009

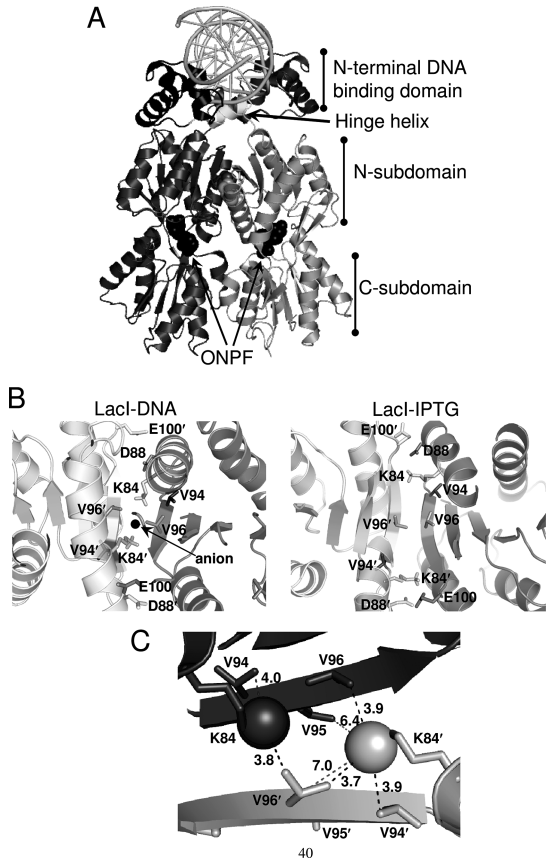

FIGURE 1: (A) Structure of the LacI dimer lacking 27 C-terminal residues bound to DNA (top, gray ladder schematic) and anti-inducer ONPF (middle, black space-filling diagram). One monomer is colored dark gray, and the other is colored in terms of individual domains. The protein is composed of the N-terminal DNA binding domain (black), the hinge helix (white), the N- and C-subdomains (light gray) with the inducer binding sites between them, and the C-terminal tetramerization domain (not present in the dimeric structure shown). The coordinates are from Protein Data Bank entry 1efa (*7*). (B) Enlarged views of the N-terminal monomer·monomer interface in the DNA-bound and inducer-bound states. Notice that the interface surrounding K84 undergoes major rearrangements in response to inducer binding (*7*). The individual residues involved in interactions with K84 are labeled. In the repressed state, K84 is buried inside a hydrophobic environment composed of V94 and V96 and other residues and is stabilized by a presumed anion (center, black dot) as well as hydrogen bonds with main chains of V94 and V96. In the induced state, K84 moves out of the interface and interacts with D88 in its own monomer and E100′ in the partner monomer. Note that the two β-sheets move closer, thus increasing the hydrophobicity of the interface in the inducer-bound state. (C) Enlarged view of the residues surrounding K84 and K84′ in the operator-bound state with the NZ groups of K84 and K84′ highlighted as enlarged spheres. The distances from V94, V95, and V96 to K84 and K84′ are shown as dashed lines (dark gray for the distances from V94 and V96 to K84 and K84′; gray for the distances from V95 to K84′). Being on the same side of the β-sheet, the γ-methyl groups of V94 and V96 are only 3.7−4.0 Å from the NZ groups of K84 and K84′; on the other hand, the distances from V95 to K84 and K84′ are 6.4 and 7.1 Å, respectively.

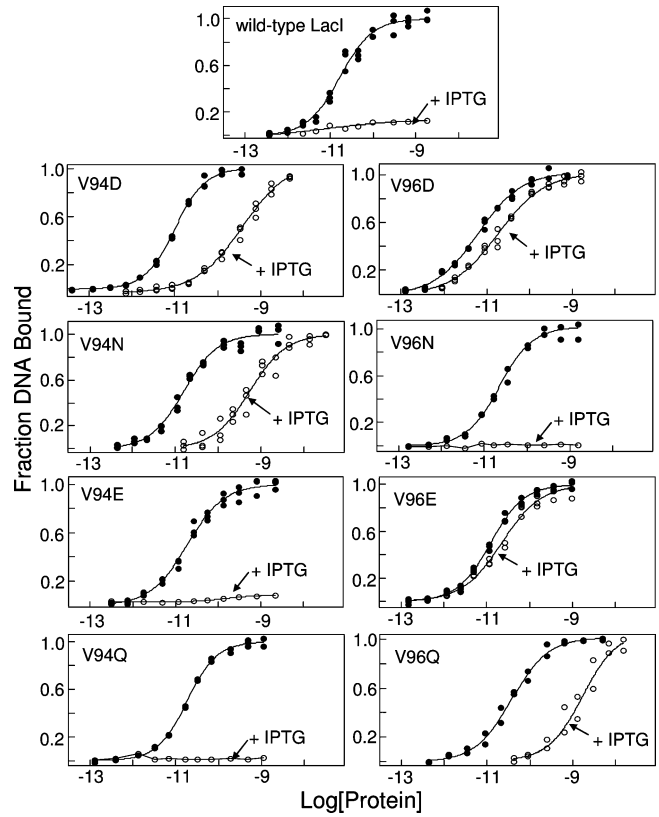

FIGURE 2: DNA (O^1) binding and inducibility of wild-type LacI and V94 and V96 mutants. Experiments were conducted as described in Materials and Methods in buffer containing 0.01 M Tris-HCl (pH 7.4), 0.15 M KCl, 0.3 mM DTT, 0.1 mM EDTA, and 5% DMSO in the absence (●) or presence (○) of IPTG. The DNA concentration was $<1.5 \times 10^{-12}$ M, and the IPTG concentration was 1 mM for all proteins except V96D and V96E, where it was 10 mM. Data shown are for single determinations (triplicate points), and the results from multiple determinations are summarized in Table 1.

that shifts between different conformational states of the repressor (*8*).

Analyses of a targeted molecular dynamics simulation of the N-subdomain motion identified three major interconnected pathways in the conformational change (*16*). Mutagenesis has disclosed further details regarding this transition (*8, 17*−*19*), and one of the residues highlighted by these studies is K84 (*8, 19, 20*). Previous work demonstrated that hydrophobic substitutions (A or L) at position 84 dramatically weakened inducer response, slowed inducer binding kinetics, and significantly increased overall protein stability (*8, 19, 20*). Crystallographic analysis of K84L showed that the hydrophobic leucine is buried deeply inside the N-subdomain interface in the unliganded state and presumably does not move from this position in response to inducer binding (*6*), accounting for the functional impact of this substitution.

Considering the fact that K84 is a buried charge in a hydrophobic interface, we asked whether providing appropriately positioned negatively charged side chains would allow ionic interactions that mimic the effects of hydrophobic substitutions at K84. In the interface, V94 and V96 are on the same side of the β-sheet as K84 and clearly approach K84 (Figure 1C). Therefore, acidic substitutions (D and E) were introduced at V94 and V96 as well as the corresponding amide derivatives (N and Q). Substitutions at V94 result in modest impacts with the shorter side chains of D and N, whereas the longer side chains of E and Q are well-tolerated. In contrast, at position 96, the negatively charged side chains impede the allosteric response to inducer to a greater degree than a completely apolar interface, and differential but much less dramatic effects are observed for their amide counterparts. Formation of a well-oriented ion pair at this subunit interface in the V96D and V96E variants weakens inducer

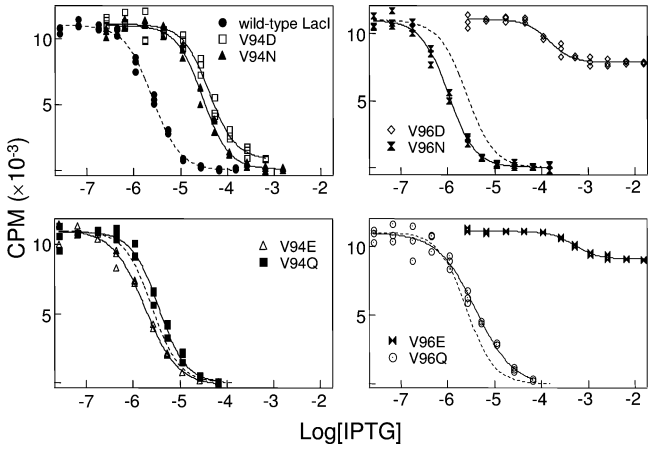

FIGURE 3: Operator release by IPTG for the wild-type protein and V94 and V96 variants. The experiments were performed as described in Materials and Methods in buffer containing 0.01 M Tris-HCl (pH 7.4), 0.15 M KCl, 0.3 mM DTT, 0.1 mM EDTA, and 5% DMSO, and with the indicated concentrations of IPTG. The operator concentration was 1.5×10^{-12} M, and protein concentrations were as follows: wild type, 2.4×10^{-10} M; V94D, 5×10^{-11} M; V94N, 6×10^{-11} M; V94E, 8.3×10^{-11} M; V94Q, 7×10^{-11} M; V96D, 3.9×10^{-11} M; V96N, 8×10^{-11} M; V96E, 1×10^{-10} M; and V96Q, 2.1×10^{-10} M. Data for a single experiment are shown (triplicate points), and the results from multiple measurements are summarized in Table 2. Dotted lines correspond to the wild-type data and are provided for comparison.

response more effectively than apolar substitution at K84 without the significant protein stabilization observed with removal of this charged side chain. Thus, properties generated by apolar substitutions at position 84 are not replicated by providing polar or ion pair interactions in the LacI monomer·monomer interface, although effective salt bridge formation can nonetheless impede allosteric response.

MATERIALS AND METHODS

Materials. The sources of chemicals and equipment used in this study are provided as they are listed.

Plasmids and Mutagenesis. Mutations were introduced into the pLS1 plasmid, which contains the *lac* repressor gene, by mutagenesis PCR using site-specific primers (Quikchange, Stratagene, La Jolla, CA) (*21, 22*). DpnI was added to the PCR product to digest template DNA. After amplification in either XL1-blue or DH5α cells, the entire LacI coding regions of the mutated plasmids were sequenced by Seqwright Inc. (Houston, TX) to ascertain that no mutations other than those designed were present.

Purification. To express LacI variant proteins, the appropriate plasmids were transformed into *Escherichia coli* BLIM cells (*21*). After being grown in 5 mL and then 50 mL cultures, the BLIM cells were further amplified in 12 L of 2× YT medium at 37 °C with shaking. After 20 h, the cells were harvested by centrifugation, resuspended in breaking buffer [200 mM Tris-HCl (pH 7.6), 200 mM KCl, 5% glucose, 10 mM magnesium acetate, and 0.3 mM DTT], and frozen at −20 °C with addition of a small amount of lysozyme (~0.5 mg/mL). Protein purification was performed as described previously (*8, 23, 24*) with the following modifications. To expedite the process and obtain highly active proteins, the post-ammonium sulfate overnight dialysis was changed to three 30 min dialyses. The purity of proteins was confirmed by SDS−PAGE (generally >95%), and the purified protein was divided into aliquots and stored at −80 °C. Protein activity, which was generally >90%, was monitored by DNA activity assays using a concentration of DNA at least 10-fold above the K_d for DNA binding.

DNA Binding. DNA binding affinities of LacI mutants were measured by nitrocellulose filter binding assays (*24, 25*). The two strands of the 40 bp wild-type operator O^1 (5′-TGTTGTGTGGAATTGTGAGCGGATAA-CAATTTCACACAGG-3′) (*26*) were purchased separately from Biosource International (Camarillo, CA), hybridized in polynucleotide kinase buffer [70 mM Tris-HCl (pH 7.6), 10 mM $MgCl_2$, and 5 mM DTT], and radiolabeled at the 5′-end using [^{32}P]ATP via a polynucleotide kinase reaction. After the labeling reaction, the unincorporated free nucleotide was removed with a Nick column (Amersham Biosciences, Uppsala, Sweden). In affinity assays, the DNA concentration was set at least 10-fold below the K_d determined for operator binding, and the protein concentration was varied as decribed in the table footnotes and figure legends. The inducer concentration was 10 mM for V96D and V96E and 1 mM for other proteins. The reaction mixtures were incubated for 20−30 min and filtered through nitrocellulose (Schleicher and Schuell, Keene, NH, or Whatman, Florham Park, NJ) to separate free DNA from protein−DNA complex. After being exposed to a phosphorimaging plate overnight, the retained protein-bound, radiolabeled DNA was then detected and quantified using a Fuji phosphorimager. Data (Y_{obs}) were analyzed with nonlinear program IgorPro (Wavemetrics) to estimate values for the variables in the following equation:

$$Y_{obs} = Y_{max}\frac{[\text{LacI}]^n}{K_d^{\,n} + [\text{LacI}]^n} + c \qquad (1)$$

where Y_{obs} and Y_{max} are the observed radioactivity at different protein concentrations and the maximal radioactivity, respectively, K_d is the apparent dissociation constant, and c is the background radioactivity from the DNA, and the value of n, the Hill coefficient, when floated was found to cluster around 1.

IPTG Binding. The inducer binding affinity of LacI mutants was measured by monitoring the total fluorescence emission intensity change at wavelengths greater than 340 nm. This intensity decreases at increasing concentrations of IPTG (*27*). The fluorescence spectra between 300 and 380 nm were collected with an excitation wavelength of 285 nm. To be at least 10-fold below the wild-type LacI K_d determined for inducer binding, the protein concentration was 1.5×10^{-7} M in monomer with the IPTG concentration varied as described in the table footnotes and figure legends. Corrected data (Y_{corr}) were analyzed with the following equation in Igor Pro (Wavemetrics) to accommodate the fluorescence signal decrease as IPTG binds:

$$Y_{corr} = Y_{max} - Y_{max}\frac{[\text{IPTG}]^n}{K_d^{\,n} + [\text{IPTG}]^n} + c \qquad (2)$$

where Y_{max}, is the total fluorescence signal change in response IPTG binding, n is the Hill coefficient for IPTG binding, K_d is the apparent equilibrium dissociation constant, and c is the fluorescence signal in the presence of a saturating concentration of IPTG. These raw data were used to calculate fraction protein bound by IPTG as reported in Figure 4.

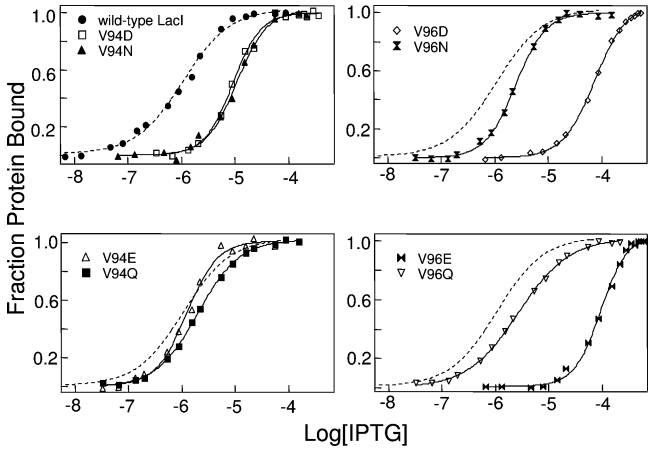

FIGURE 4: Fluorescence measurements of IPTG binding properties for wild-type LacI and V94 and V96 mutants. The buffer consisted of 0.01 M Tris-HCl (pH 7.4) and 0.15 M KCl. The experiments were conducted as described in Materials and Methods. Data are shown for single determinations, and the results from multiple determinations are summarized in Table 2.

The method described above depends primarily on the fluorescence signal change of W220 in the repressor, which may be different in LacI variants. To confirm the binding properties of LacI variants, inducer binding for several mutants was assessed using a filter binding method with [^{14}C]IPTG (~0.1 μM) (derived from ref *28*), which was incubated with increasing concentrations of LacI variants (above the K_d of wild-type LacI measured by fluorescence) as well as cold IPTG (100 μM) in duplicate to provide background values and filtered through nitrocellulose. The remainder of the procedure is similar to the filter binding assay for DNA binding, except that the data were fit with a linear equation. Analogous to activity assessment of DNA binding, this assay is near the stoichiometric range for wild-type LacI, but not for the variants with lower affinity. This method provides an assessment of relative IPTG binding affinities for the various mutants.

Operator Release. In these experiments, repressor was first incubated with operator to form the LacI·DNA complex, and then increasing concentrations of IPTG were added to release the operator from the LacI·DNA complex. The concentration of radiolabeled DNA was 1.5×10^{-12} M; the repressor concentration was set to produce ~80−90% saturation of protein by operator DNA (*8, 17*), and the concentration of inducing sugar was varied as indicated in table footnotes and figure legends. After assessment of radiolabel bound with a Fuji phosphorimager, the data were analyzed with eq 2 by replacing K_d with $[IPTG]_{mid}$. Since operator release involves at least two events, (1) binding of inducer molecules and (2) the accompanying protein conformational change leading to operator release, the $[IPTG]_{mid}$ can be used only to compare the properties of different proteins since this value is not a true equilibrium constant but a composite assessment of multiple events.

Urea Denaturation. Urea denaturation experiments were conducted by monitoring changes in fluorescence intensity at 340 nm (mainly from W220) with increasing concentrations of urea (made fresh daily) (*10, 23*). The protein concentration was 2×10^{-6} M in monomer. Tetrameric repressors were allowed to incubate with urea at room temperature before fluorescence spectra were recorded. Varying incubation times were employed to ensure that equilibrium was achieved. To confirm the results by fluorescence, the circular dichroism signal at 222 nm of selected samples was also monitored. The urea solution concentration was confirmed by refractometry (*29, 30*). Data were analyzed as described in refs *30* and *31* to extract the midpoint of the transition, ΔG^{o}_{N-U}, and m values for comparison with those of the wild-type repressor. These analyses presumed that there are only two states (native and unfolded) in the transition region and that the reaction is reversible. Previous work has shown these presumptions apply to wild-type LacI and that the transition measured is unfolding to tetramer tethered at the C-terminus (*10*). Replicates for each protein, including both fluorescence and circular dichroism data, were fit globally to minimize the errors in data analyses.

Pymol Analysis. To model the potential structures of the interface mutants, the mutagenesis function in Pymol was used. To assess the structural effects of introduced substitutions, Pymol executes a simple annealing simulation to avoid potential steric clashes and usually displays two configurations with the highest probability: one structure is based on a backbone-dependent model, whereas the other is calculated using a backbone-independent model. The model with higher probability is shown.

RESULTS

Operator Binding of Mutations at V94 and V96. To explore whether ion pair formation might affect LacI function, negatively charged residues D and E and their derivative amides N and Q were introduced at interface positions 94 and 96 via site-specific mutagenesis. The resulting mutant proteins were purified by ammonium sulfate precipitation followed by phosphocellulose column chromatography, with elution profiles characteristic of well-folded, tetrameric LacI.

O^1 binding affinities of variant proteins were determined in the absence of inducer using nitrocellulose filter binding [Figure 2 (filled symbols) and Table 1] (*25*). Variants at position 94 exhibited DNA binding affinities comparable to those of wild-type LacI. The acidic substitutions at V96 (V96D and V96E) bind DNA slightly tighter than wild-type LacI, whereas the amide derivatives, V96N and V96Q, have a slightly lower DNA binding affinity. These observed operator binding behaviors are very consistent with the phenotypes previously identified for each of these substitutions (Table 1) (*32*).

Inducibility of Interface Mutants. For wild-type LacI, the operator binding affinity is decreased ~4 orders of magnitude by inducer binding (*8, 24*). At position 94, the longer side chain substitutions, V94E and V94Q, are very similar to wild-type LacI. In contrast, the shorter side chain substitutions, V94D and V94N, diminish the allosteric response, with affinities that are decreased by only 2 orders of magnitude. At position 96, the neutral V96N mutant behaves like wild-type LacI, and the V96Q mutation reduces the magnitude of K_d change by ~20-fold. In contrast, the response to inducer for the charged side chains, V96D and V96E, is effectively abolished (Figure 2 and Table 1). These V96D and V96E results suggest that formation of a strong ion pair can impede allosteric response, behavior similar to that of

Table 1: Operator O^1 Binding Properties and Inducibilities of Interface Variants[a]

	K_d ($\times 10^{-11}$ M)	mutant/WT	with IPTG[b] ($\times 10^{-11}$ M)	(with IPTG)/(without IPTG)	phenotype[c]
wild-type LacI	1.5 ± 0.4		>10000	>1000	+
V94D	1.0 ± 0.1	0.7 ± 0.1	**36 ± 4**	**36 ± 4**	ND[d]
V94N	1.4 ± 0.2	0.9 ± 0.2	**63 ± 14**	**45 ± 6**	ND[d]
V94E	2.0 ± 0.1	1.3 ± 0.2	>10000	>1000	+r
V94Q	1.8 ± 0.1	1.2 ± 0.1	>10000	>1000	+
V96D	0.8 ± 0.2	0.5 ± 0.2	**1.9 ± 0.2**	**2.3 ± 0.7**	ND[d]
V96N	2.6 ± 0.3	1.7 ± 0.2	>10000	>1000	ND[d]
V96E	0.8 ± 0.2	0.6 ± 0.2	**1.1 ± 0.3**	**1.3 ± 0.3**	+s
V96Q	3.7 ± 0.3	2.5 ± 0.3	**150 ± 40**	**41 ± 3.1**	+s
K84A[e]	3.3 ± 0.8	2.2 ± 0.4	22 ± 2	**6.7 ± 1.6**	+s
K84L[e]	**23 ± 3**	**15 ± 2**	110 ± 5	**4.8 ± 0.6**	±s

[a] Values shown represent the average and standard deviation from a minimum of three measurements and up to five measurements. Values for mutant proteins that deviate significantly from the wild-type value are in bold print. Operator binding experiments were performed in buffer containing 0.01 M Tris-HCl (pH 7.4), 0.15 M KCl, 0.3 mM DTT, 0.1 mM EDTA, and 5% DMSO. [b] The operator concentration was below 1.5×10^{-12} M. Where present, the IPTG concentration was 10 mM for V96D and V96E and 1 mM for all other proteins. [c] Data from ref *32*: +, >200-fold repression; ±, 20−200-fold repression; s, I^s phenotype (insensitive to inducer); r, heat resistance. [d] No data available. [e] From ref *8*.

Table 2: Inducer Binding Properties of Interface Mutants[a]

	$[IPTG]_{mid}$ ($\times 10^6$ M) for operator release[b]	mutant/WT	relative % release[c]	$K_{R/I}$ ($\times 10^6$ M)[d]	Hill coefficient	$[IPTG]_{mid}/K_{R/I}$
wild-type LacI	2.9 ± 0.6		100	1.2 ± 0.1	1.0 ± 0.1	2.4 ± 0.3
V94D	**34 ± 6**	**12 ± 2**	93	**10 ± 1**	**1.7 ± 0.1**	3.4 ± 0.5
V94N	**29 ± 2**	**10 ± 2**	96	**12 ± 1**	**1.9 ± 0.4**	2.4 ± 0.2
V94E	2.4 ± 0.6	0.8 ± 0.2	99	1.4 ± 0.1	**1.6 ± 0.2**	1.7 ± 0.2
V94Q	3.3 ± 0.2	1.1 ± 0.1	100	1.8 ± 0.3	**1.3 ± 0.2**	1.8 ± 0.3
V96D	**120 ± 20**	**41 ± 4**	**29**	**68 ± 3**	**1.5 ± 0.1**	1.8 ± 0.2
V96N	1.3 ± 0.4	0.5 ± 0.1	100	2.0 ± 0.4	**1.5 ± 0.1**	0.7 ± 0.2
V96E	**630 ± 100**	**220 ± 20**	**18**	**96 ± 9**	**1.4 ± 0.1**	**6.6 ± 0.5**
V96Q	3.9 ± 0.3	1.3 ± 0.2	98	3.3 ± 0.7	1.0 ± 0.1	1.2 ± 0.3
K84A[e]	2.3 ± 0.6	0.8 ± 0.2	**~50**	1.4 ± 0.2		1.6 ± 0.3
K84L[e]	1.7 ± 0.2	0.6 ± 0.1	**~50**	1.4 ± 0.2		1.2 ± 0.2

[a] Values shown represent the average and standard deviation from a minimum of three measurements and up to six measurements. Values for mutant proteins that deviate significantly from the wild-type value are in bold print. [b] Operator release experiments were performed in buffer containing 0.01 M Tris-HCl (pH 7.4), 0.15 M KCl, 0.3 mM DTT, 0.1 mM EDTA, and 5% DMSO. The protein concentrations were as follows: wild type, 2.4×10^{-10} M; V94D, 5×10^{-11} M; V94N, 6×10^{-11} M; V94E, 8.3×10^{-11} M; V94Q, 7×10^{-11} M; V96D, 3.9×10^{-11} M; V96N, 8×10^{-11} M; V96E, 1×10^{-10} M; and V96Q, 2.1×10^{-10} M. [c] This ratio is the percentage of operator released by mutant relative to wild type. [d] IPTG binding experiments were conducted in buffer containing 0.01 M Tris-HCl (pH 7.4) and 0.15 M KCl. [e] From ref *8*.

K84A and K84L substitutions that eliminate buried charge and enhance hydrophobicity. The normal inducer response of V94E and the partial response of V94D suggest that precise geometry may be necessary for formation of an effective ion pair, as Kumar and Nussinov previously pointed out for other systems (*33*).

To further assess the effects of the interface substitutions on the allosteric transition, operator release was monitored for the mutants (*8, 17*). The release experiments measure both how much inducer is required to release operator from the operator·protein complex and the extent of operator release, providing a crude measurement of the allosteric response in LacI variants (Figure 3 and Table 2). As observed for operator binding, the short and long side chains behave differently at position 94: $[IPTG]_{mid}$ is ~10-fold higher for V94D and V94N but near wild-type values for V94E and V94Q. At position 96, the charged and neutral side chains again exhibit different behaviors: D and E substitutions increase $[IPTG]_{mid}$ and diminish the extent of release to ~20−30%. V96N behaves like wild-type LacI, and V96Q, despite a higher affinity in the presence of inducer, shows full release of operator DNA. For those mutant proteins with a diminished level of release, to assess the potential for slower inducer binding kinetics affecting this parameter, the protein·DNA complex was incubated for longer time periods (up to 4 h) before being filtered through a nitrocellulose membrane. These experiments generated similar $[IPTG]_{mid}$ values.

Inducer Binding of Interface Mutants. The inducer binding affinities of the interface mutants were monitored by fluorescence spectroscopy to correlate with release experiments. The results are consistent with previous patterns, with position 94 behavior correlating with side chain length and position 96 behavior correlating with charge (Figure 4 and Table 2). Inducer binding affinity is similar to that for wild-type LacI for V94E and V94Q but is decreased by ~10-fold for V94D and V94N. Small decreases are observed for the N and Q amide substitutions at V96, whereas a significantly greater decrease (60−80-fold) is observed for the acidic V96D and V96E substitutions. Because K84A and K84L exhibit substantially decreased kinetic constants, despite wild-type equilibrium parameters, rate measurements confirmed that this parameter did not account for the decreased affinity observed, particularly for V96D and V96E. Note that the two mutants (V96D and V96E) that have very elevated $[IPTG]_{mid}$ values also have a significantly higher K_d for inducer ($K_{R/I}$). Inducer binding to LacI in the absence of DNA is noncooperative, with a Hill coefficient of 1. Notably, all variants, except V96Q, exhibit increased cooperativity of inducer binding (Table 2).

Operator release involves both inducer binding affinity and the consequent allosteric transition, a relationship that can be quantitatively assessed by the ratio between the $[IPTG]_{mid}$ of operator release and $K_{R/I}$ (or allosteric ratio) (Table 2). This ratio may reflect the capability of the repressor protein to undergo the IPTG-induced conformational change. This

Table 3: Fluorescence Properties of Interface Variants[a]

	emission maximum without IPTG (nm)	emission maximum with IPTG (nm)[b]	shift (nm)
wild-type LacI	340 ± 1	330 ± 2	10
V94D	346 ± 2	337 ± 2	9
V94N	343 ± 2	334 ± 1	9
V94E	340 ± 2	330 ± 1	10
V94Q	340 ± 1	330 ± 2	10
V96D	344 ± 1	335 ± 2	9
V96N	339 ± 1	333 ± 1	6
V96E	344 ± 1	334 ± 1	10
V96Q	340 ± 2	333 ± 2	7

[a] These numbers represent the average and standard deviation from 11−15 spectra. Fluorescence spectra were recorded in buffer containing 0.01 M Tris-HCl (pH 7.4) and 0.15 M KCl. Note that the emission peak was red-shifted for V94D, V94N, V96D, and V96E both in the presence and in the absence of inducer. Smaller shifts in fluorescence spectrum maxima were observed for V96N and V96Q. [b] In the presence of 1 mM IPTG.

ratio is 2.4 for wild-type LacI. The shorter side chain substitutions, N and D, at V94 display values similar to or slightly above that for wild-type LacI, whereas the longer side chain substitutions, E and Q, exhibit ratios slightly lower than that of wild-type LacI. The polar amide derivatives at position 96, V96N and V96Q, have ratios somewhat lower than that of the wild type, whereas the acidic V96E substitution has a value significantly higher than that observed for wild-type LacI. Interestingly, V96D (also acidic), which has an $[IPTG]_{mid}$ much greater than that for wild-type LacI, has a similar allosteric ratio, suggesting that the changed operator release may be due primarily to weakened inducer binding.

Changes in the emission maximum and shape of the fluorescence spectra were observed for V94D, V94N, V96D, V96E, sorting as described previously into a pattern where chain length impacts behavior at position 94 and charge at position 96 (Table 3). Because these alterations could conceivably impact measurement of inducer binding using Trp 220 fluorescence (*27*), we confirmed the affinities assessed by fluorescence spectroscopy by directly assessing [^{14}C]IPTG interaction (data not shown). These experiments using nitrocellulose trapping of the protein−IPTG complex provide comparative measurements, but the conditions do not allow precise determination of the binding constants. Nonetheless, the [^{14}C]IPTG binding pattern observed for the variants relative to wild-type LacI correlates very well with the data reported in Figure 4 and Table 2.

Stability of the V94 and V96 Mutants. For a thermodynamically linked system, protein stability can affect ligand binding and influence the allosteric transition of the repressor. Wild-type LacI exhibits a concerted process of folded tetramer to unfolded monomers (*10*). Previous work on K84A and K84L has shown that stability was dramatically altered when K84 was substituted with alanine or leucine (*8, 19, 20*), attributed primarily to the improved hydrophobic packing in the N-subdomain monomer·monomer interface (*6*). In contrast, polar and charged substitutions at V94 and V96 all diminish protein stability to varying degrees (Figure 5 and Table 4) as measured by urea denaturation experiments. Analysis of ΔG^{o}_{N-U} and *m* values (Figure 5B) utilized data from both fluorescence and circular dichroism measurements, with the assumptions noted in Materials and Methods. For V94D, a biphasic unfolding pattern was observed at shorter

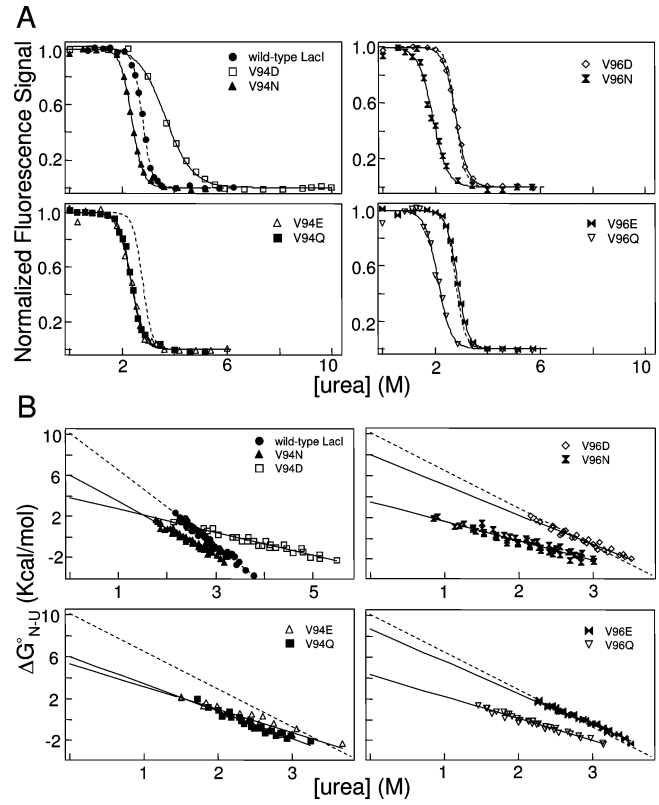

FIGURE 5: Urea denaturation of wild-type LacI and V94 and V96 mutant proteins. The experiments were conducted as described in Materials and Methods in buffer containing 0.01 M Tris-HCl (pH 7.5) and 0.1 M K_2SO_4. The protein concentration was 2×10^{-6} M in monomer. In panel A, the data were fit only for the purpose of determining the midpoint values reported for multiple experiments in Table 4. The dotted line in each panel corresponds to wild-type LacI. Panel B shows global fitting of the denaturation data (including both fluorescence and circular dichroism data) for protein variants for calculation of the unfolding free energy (ΔG°_{N-U}) and *m* value. The data were analyzed using the linear extrapolation method with a linear extrapolation to zero urea to calculate the ΔG°_{N-U} (*31*). The fit for wild-type LacI is represented as a dashed line in each panel for comparison.

Table 4: Unfolding of Interface Variants[a]

	$[urea]_{mid}$[b]	ΔG°_{N-U}[c]	*m*[c]
wild-type LacI	2.8 ± 0.1	10 ± 0.6	3.6 ± 0.2
V94D	3.6 ± 0.3	3.8 ± 0.2	1.1 ± 0.1
V94N	2.4 ± 0.1	6.0 ± 0.2	2.6 ± 0.1
V94E	2.3 ± 0.1	5.3 ± 0.3	2.2 ± 0.1
V94Q	2.3 ± 0.1	6.0 ± 0.4	2.6 ± 0.2
V96D	2.8 ± 0.1	8.0 ± 0.3	2.9 ± 0.1
V96N	1.9 ± 0.1	3.5 ± 0.2	1.9 ± 0.1
V96E	2.8 ± 0.1	8.7 ± 0.2	3.1 ± 0.1
V96Q	2.1 ± 0.1	4.3 ± 0.2	2.1 ± 0.1
K84A[d]	>6		
K84L[d]	>6		

[a] Values shown represent the average and standard deviation for a minimum of three measurements and up to five measurements. [b] Urea experiments were performed in buffer containing 0.01 M Tris-HCl (pH 7.5) and 0.15 M K_2SO_4. The urea solution was made fresh daily. [c] ΔG°_{N-U} and *m* values were globally calculated as described in refs *30* and *31* using multiple data sets. [d] For K84A and K84L, the transition is not complete even at 8 M urea; therefore, the $[urea]_{mid}$ cannot be estimated accurately. Data were taken from ref *20*.

times, collapsing to a single transition with long incubation. Although a higher urea concentration is necessary to unfold V94D, the ΔG^{o}_{N-U} and *m* values are lower than those for the wild-type protein, a situation that could arise due to

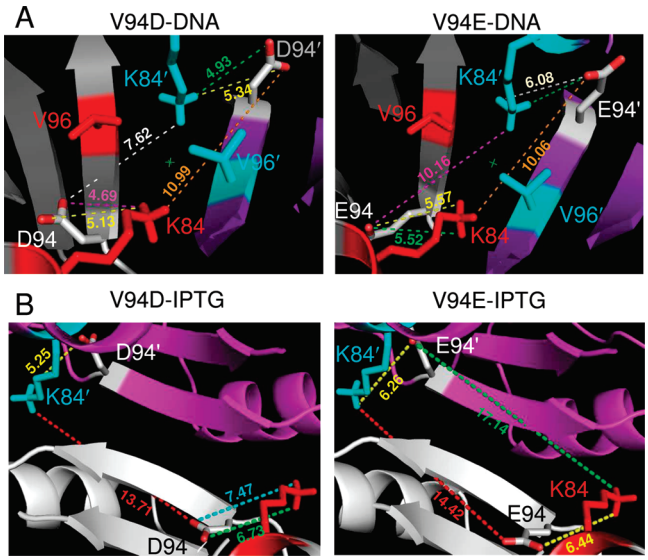

FIGURE 6: Interface structures for V94 variants. Substituted N-subdomain monomer•monomer interface of V94D and V94E in the DNA-bound (A) (Protein Data Bank entry 1efa) and inducer-bound (B) forms (Protein Data Bank entry 1lbh) (*7, 14*). Note that the presumed anion is represented by a green cross. These potential structures were generated using the mutagenesis function in PyMol (http://pymol.sourceforge.net). The distances between acidic substitutions and K84 are shown with labeled dashed lines (the numbers beside the dashed lines are the distances in angstroms). Note that there is no obvious electrostatic contact formed between D or E at position 94 and K84′ in either DNA- or inducer-bound form. The side chain carboxyl at position 94 appears closest to K84 within the same monomer.

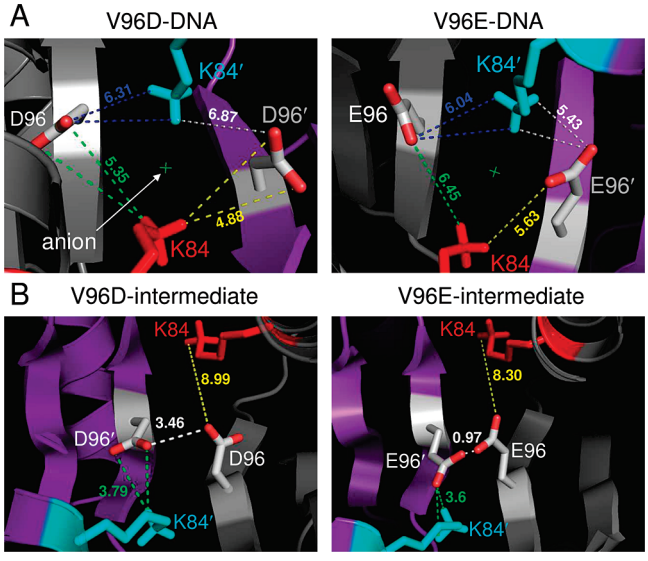

FIGURE 7: Interface structures for V96 variants. The substituted N-subdomain monomer•monomer interface for V96 in the DNA-bound form is shown in panel A with the presumed anion represented by a green cross (Protein Data Bank entry 1efa) (*7*). These theoretical structures were generated using the mutagenesis function in PyMol. The dashed lines represent the distances between indicated residues (the numbers beside the dashed lines are the distances in angstroms). Note that these structures suggest a well-formed electrostatic network between acidic substitutions at positions 96 and 96′ and positions 84 and 84′. Since IPTG has no effect on operator binding, we presume that the structure would be similar for the IPTG-bound state, which is not shown. Intermediate (500 ps in a 900 ps transition) structures in the TMD pathway (*16*) (B) demonstrate that the negative charges at D96 and D96′ and at E96 and E96′ are very close in the intermediate state, potentially inhibiting the allosteric transition pathway.

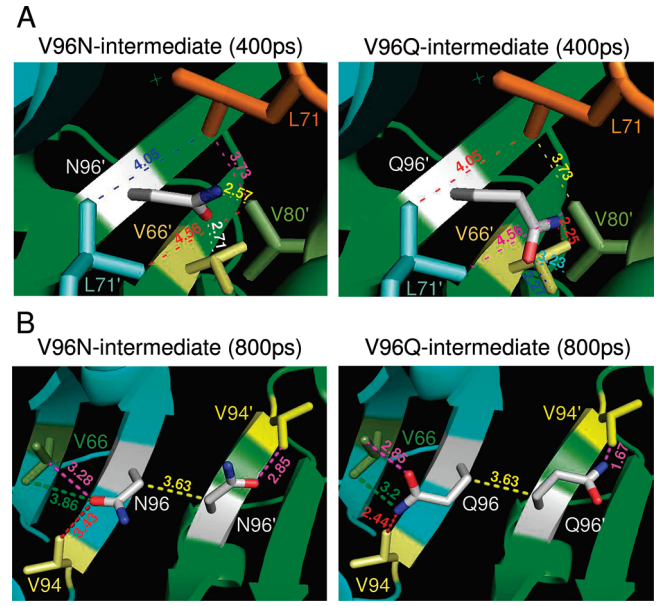

FIGURE 8: Structures for V96N and V96Q at intermediate times in the TMD pathway (*16*). Panel A shows 400 ps intermediate structures with the polar side chain of Q96 in the proximity of the surrounding hydrophobic groups (V66, L71, and V80), and these residues are even closer for N96. Panel B shows a later intermediate (800 ps) near the end of the transition. The longer side chains of Q96 are even closer to V94 and V66 than when the distance is calculated for N96. This crowding in the interface coupled with the absence of attractive forces may account for the diminished stability of these two protein variants compared to their charged counterparts.

violation of the two-state assumptions in the analysis. The remaining substitutions at position 94 diminished both $\Delta G°$ and *m* values. In contrast, V96D and V96E exhibit small decreases in both $\Delta G°$ and *m* values, with V96E closest to wild-type behavior. V96N and V96Q exhibit stability and *m* values lower than those of wild-type LacI or their charged counterparts. These patterns largely track with the other behaviors of this series of mutations. Note that, despite the diminished stability to urea denaturation, all the variants examined are sufficiently stable to maintain quaternary structure required for operator binding at concentrations down to $\sim 10^{-11}$ M.

Modeling the Subunit Interface Structure. To identify possible interactions that influence function, we used PyMol to generate IPTG-bound and DNA-bound structures for the mutant proteins. These models presume that the side chains in the D and E variants at positions 94 and 96 are charged. This assumption is strengthened by the observed charge on the side chain of K84/K84′, which is buried with an anion and water in the monomer•monomer interface in the DNA-bound structure (*7, 14*).

These calculated structures show no pattern that would be consistent with a salt bridge network between the acidic residues at positions 94/94′ and K84/K84′ in either the DNA- or IPTG-bound states (Figure 6). Generally, the side chain at position 94 interacts with K84 within the same chain. The longer side chains of E and Q at position 94 employ the β- and γ-carbons in apolar interactions, similar to wild-type V94. These apolar interactions may promote normal inducer binding and response, but the predicted locations of the polar and charged moieties on the amide and carboxyl groups provide a structural rationale for diminishing the stability of

the interface, and thereby the overall protein (e.g., refs *34* and *35*). The shorter D and N side chains offer lower potential for apolar interactions and thus deplete the apolar interface, accounting for the diminished stability of these proteins. How this arrangement contributes to other features of V94D and V94N, e.g., decreased affinity for IPTG and weaker inducer response, is less apparent, although rearrangements in the subunit interface could influence all these parameters.

In contrast, substitution at position 96 with either D or E results in a well-formed cross-subunit electrostatic interaction relay system in the predicted structure for the DNA-bound form (Figure 7A). The acidic side chains at positions 96 and 96′ are predicted to interact with the basic K84 and K84′ side chains, with distances of 5−6 Å. This set of interactions would impede the IPTG-induced transition and appears to promote stability to near-wild-type $\Delta G°$ and m values for urea-induced unfolding for V96D and V96E substitutions, consistent with the experimental data.

Intermediate steps of the allosteric transition simulated by TMD (*16*) were also explored for the V96 variants. At a point approximately midway (500 ps out of 900 ps) in this transition, the positions of the acidic side chains for D and E substitutions at positions 96 and 96′ would be within a few angstroms of one another (Figure 7B). The anticipated charge−charge repulsion would impede formation of this intermediate, suggesting an additional contribution for the lack of IPTG-induced transition in V96D and V96E. The greater crowding for E96•E96′ suggests that the structure has less flexibility and may explain the higher allosteric ratio ($[IPTG]_{mid}/K_{R/I}$) for V96E.

For the N and Q substitutions at position 96, at points in the intermediate structures, the polar groups move close to V80 (∼2.3−3 Å), which forms part of a hydrophobic patch that includes V66 and L71 within each subunit (Figure 8). This proximity between polar and hydrophobic groups could contribute to the lower stability of N and Q substitutions at position 96. The length of the Q side chain and the consequent crowding in the intermediate structures, especially with V94 in this region (Figure 8B), may lead to the weakened inducer response (i.e., increased affinity for operator in the presence of inducer) observed for V96Q.

DISCUSSION

An integrated overview of individual properties discloses substantial differences between properties for the acidic and amide substitutions at V94 and V96 and the K84A and K84L mutants (Table 5). None of the V94 and V96 variants exhibits overall behavior similar to that of the K84A and K84L proteins. Rather, this set of proteins displays distinct variations that follow a consistent theme. (i) The shorter side chains at position 94 compromise inducer binding and weaken the inducer response, whereas the longer side chains have a minimal impact. (ii) The acidic side chains at position 96 abolish allosteric response and impede DNA release, whereas the amide derivatives behave like wild-type LacI. All substitutions diminish stability, with the V96 acidic variants having the smallest impact. In contrast, K84A and K84L proteins feature enhanced stability, impaired allosteric response, a significantly decreased rate of inducer binding, and wild-type IPTG binding affinity (*8, 19, 20*). These distinctions demonstrate that ion pair formation within the hydrophobic monomer•monomer interface does not replicate the impact of enhanced hydrophobic character.

Of the ionizable residues in a protein, including lysine, only a small percentage is found buried, and the fraction ionized diminishes with the extent of burial, whether in a protein monomer or a subunit interface (*36*). Substantial shifts in pK_a can accompany burial of charged side chains, and the role of side chain ionization and ionic interactions in protein structure and folding has been widely explored (*33−35, 37−41*). Single substitutions with ionizable amino acids in a critical region can affect folding, destabilizing the native structure and favoring the unfolded state (*34, 37*). In staphylococcal nuclease, for example, the majority of buried basic and acidic residues are uncharged, with pK_a shifts of up to 5 units to achieve this neutrality (*37*). However, similar to the behavior of K84 at the LacI subunit interface, the buried side chain of staphylococcal nuclease variant L38K is charged (*37*). Detailed measurements for this protein indicate that water penetration to hydrate the ionized amino groups and nondisruptive structural rearrangements that promote this hydration are key elements in stabilizing this buried side chain (*37*). Similarly, K84 in LacI has a solvent anion and water buried in the subunit interface (*7, 14*).

In Arc repressor, substitution of a buried salt bridge triad with an apolar grouping resulted in enhanced stability, demonstrating the penalty exacted by buried ionic networks (*41*), a phenomenon also observed in other systems (*4, 35, 42*). Even so, the formation of salt bridge networks and cooperativity of electrostatic interactions can enhance the stability of buried ionic interactions in proteins (*43−45*). In contrast

Table 5: Overall Properties of Interface Variants[a]

protein	operator affinity	inducer response[b]	IPTG midpoint for release	fluorescence maximum altered	IPTG binding K_d	allosteric ratio	urea stability
V94D	∼	↓	↑	√	↑	∼	⇊
V94N	∼	↓	↑	√	↑	∼	↓
V94E	∼	∼	∼	∼	∼	∼	↓
V94Q	∼	∼	∼	∼	∼	∼	↓
V96D[c]	∼	⇊	⇈; ⇊%	√	⇈	∼	∼
V96N	∼	∼	∼	∼	∼	∼	⇊
V96E[c]	∼	⇊	⇈; ⇊%	√	⇈	↑	∼
V96Q	∼	↓	∼	∼	∼	∼	⇊
K84A[d]	∼	↓	∼; ↓%	∼	∼	∼	⇈
K84L[d]	↓	↓	∼; ↓%	∼	∼	∼	⇈

[a] All the symbols are relative to the value of wild-type LacI: ∼, within ∼2.5-fold of the wild-type LacI parameter (except for urea stability); ↑, increased; ⇈, significantly increased; ↓, decreased; ⇊, significantly decreased; √, yes. [b] Inducer response indicates the ratio of operator binding K_d in the presence and absence of inducer [(with IPTG)/(without IPTG)] in Table 1. [c] ⇊% means that the percentage of operator release (Table 2) is decreased substantially. [d] From refs *8* and *20*.

to charged residues, burial of polar residues generally exacts a smaller energy burden, with the cost apparently modulated by the large number of hydrogen bond partners available in the protein interior (*40*).

Introducing an ionized side chain into a position where it can "toggle" between internal and solvent-exposed environments provides a general mechanism for exerting significant influence on both structure and function. In LacI, the positively charged K84 side chains within the monomer·monomer interface are buried in the DNA-bound structure, and the consequent energetic penalty is modulated, at least in part, by the burial of an accompanying solvent anion and water (*7, 14*). Nonetheless, the presence of this charged network within a hydrophobic region destabilizes the interface to allow facile rearrangement in response to binding at a remote site; that is, the system is poised for LacI allosteric transition in response to inducer. When triggered by the structural changes that accompany IPTG binding, the stabilizing but mobile anion allows these charged lysine residues to shift to a more solvent-exposed position, with consequent coalescence of the apolar subunit interface (*7, 14*). In this scenario, buried charge is functionally quite important, and the ionized state of the lysine side chain is critical to an effective "switching" mechanism for altering function in response to stimuli from a wide range of interactions.

An interesting question is whether lysine has unique attributes for serving as a trigger for such a switching mechanism. The apolar regions within both lysine and arginine side chains, longer than either glutamate or aspartate, offer stabilizing interactions in a hydrophobic environment. However, the charged amino group is significantly less bulky than the guanidino moiety of arginine, and the longer aliphatic region of lysine enhances hydrophobic character, suggesting significant differences between these amino acids for both structure and function. As an example, in studies of staphylococcal nuclease variants with substitution of a V66 with all ionizable amino acids, only arginine induces a structural change to expose the charged side chain to water (*34*). Behavior by and induced by buried lysines in proteins (*34, 37*−*39*) and the effects of substitutions on LacI function suggest that buried (or partially buried) lysines, with the capacity to occupy disparate environments in different states, can serve a pivotal role not only in protein folding but also in assembly and allosteric response.

The experiments presented in this study demonstrate that an ion pair formed with lysine in an apolar environment does not replicate changes that eliminate side chain charge and enhance the hydrophobic character. However, a well-positioned, buried ion network can impede conformational changes critical to normal function, as observed for V96D and V96E. In the case of LacI, the charged K84 side chain and the surrounding hydrophobic environment play crucial roles, illustrating that a delicate balance of charge versus hydrophobicity is pivotal in achieving the precise degree of destabilization at the monomer·monomer interface to support the multiple functions of LacI.

ACKNOWLEDGMENT

We thank Dr. Liskin Swint-Kruse (The University of Kansas Medical Center) for critical reading of the manuscript and always illuminating comments and discussion as well as general gifts of some Protein Data Bank files of TMD simulations, Kevin Kam for assistance with some IPTG binding experiments, Anishika D'Souza for help with experiments, and members of the Matthews laboratory for useful discussions and effective feedback.

REFERENCES

1. Baldwin, R. L. (2007) Energetics of protein folding. *J. Mol. Biol. 371*, 283–301.
2. Nakamura, H. (1996) Roles of electrostatic interaction in proteins. *Q. Rev. Biophys. 29*, 1–90.
3. Cornilescu, G., Lee, B. R., Cornilescu, C. C., Wang, G., Peterkofsky, A., and Clore, G. M. (2002) Solution structure of the phosphoryl transfer complex between the cytoplasmic A domain of the mannitol transporter $II^{Mannitol}$ and HPr of the *Escherichia coli* phosphotransferase system. *J. Biol. Chem. 277*, 42289–42298.
4. Hendsch, Z. S., and Tidor, B. (1994) Do salt bridges stabilize proteins? A continuum electrostatic analysis. *Protein Sci. 3*, 211–226.
5. Kajander, T., Kahn, P. C., Passila, S. H., Cohen, D. C., Lehtio, L., Adolfsen, W., Warwicker, J., Schell, U., and Goldman, A. (2000) Buried charged surface in proteins. *Structure 8*, 1203–1214.
6. Bell, C. E., Barry, J., Matthews, K. S., and Lewis, M. (2001) Structure of a variant of *lac* repressor with increased thermostability and decreased affinity for operator. *J. Mol. Biol. 313*, 99–109.
7. Bell, C. E., and Lewis, M. (2000) A closer view of the conformation of the Lac repressor bound to operator. *Nat. Struct. Biol. 7*, 209–214.
8. Swint-Kruse, L., Zhan, H., and Matthews, K. S. (2005) Integrated insights from simulation, experiment, and mutational analysis yield new details of LacI function. *Biochemistry 44*, 11201–11213.
9. Matthews, K. S., and Nichols, J. C. (1998) Lactose repressor protein: Functional properties and structure. *Prog. Nucleic Acid Res. Mol. Biol. 58*, 127–164.
10. Barry, J. K., and Matthews, K. S. (1999) Thermodynamic analysis of unfolding and dissociation in lactose repressor protein. *Biochemistry 38*, 6520–6528.
11. Monod, J., Wyman, J., and Changeux, J. P. (1965) On the nature of allosteric transitions: A plausible model. *J. Mol. Biol. 12*, 88–118.
12. Wilson, C. J., Das, P., Clementi, C., Matthews, K. S., and Wittung-Stafshede, P. (2005) The experimental folding landscape of monomeric lactose repressor, a large two-domain protein, involves two kinetic intermediates. *Proc. Natl. Acad. Sci. U.S.A. 102*, 14563–14568.
13. Wilson, C. J., Zhan, H., Swint-Kruse, L., and Matthews, K. S. (2007) The lactose repressor system: Paradigms for regulation, allosteric behavior and protein folding. *Cell. Mol. Life Sci. 64*, 3–16.
14. Lewis, M., Chang, G., Horton, N. C., Kercher, M. A., Pace, H. C., Schumacher, M. A., Brennan, R. G., and Lu, P. (1996) Crystal structure of the lactose operon repressor and its complexes with DNA and inducer. *Science 271*, 1247–1254.
15. Friedman, A. M., Fischmann, T. O., and Steitz, T. A. (1995) Crystal structure of *lac* repressor core tetramer and its implications for DNA looping. *Science 268*, 1721–1727.
16. Flynn, T. C., Swint-Kruse, L., Kong, Y., Booth, C., Matthews, K. S., and Ma, J. (2003) Allosteric transition pathways in the lactose repressor protein core domain: Asymmetric motions in homodimer. *Protein Sci. 12*, 2523–2541.
17. Swint-Kruse, L., Zhan, H., Fairbanks, B. M., Maheshwari, A., and Matthews, K. S. (2003) Perturbation from a distance: Mutations that alter LacI function through long-range effects. *Biochemistry 42*, 14004–14016.
18. Barry, J. K., and Matthews, K. S. (1999) Substitutions at Histidine 74 and Aspartate 278 alter ligand binding and allostery in lactose repressor protein. *Biochemistry 38*, 3579–3590.
19. Chang, W.-I., Olson, J. S., and Matthews, K. S. (1993) Lysine 84 is at the subunit interface of *lac* repressor protein. *J. Biol. Chem. 268*, 17613–17622.
20. Nichols, J. C., and Matthews, K. S. (1997) Combinatorial mutations of *lac* repressor. Stability of monomer-monomer interface is increased by apolar substitution at position 84. *J. Biol. Chem. 272*, 18550–18557.

21. Wycuff, D. R., and Matthews, K. S. (2000) Generation of an AraC-araBAD promoter-regulated T7 expression system. *Anal. Biochem. 277*, 67–73.
22. Chen, J., and Matthews, K. S. (1992) Deletion of lactose repressor carboxyl-terminal domain affects tetramer formation. *J. Biol. Chem. 267*, 13843–13850.
23. Chen, J., and Matthews, K. S. (1994) Subunit dissociation affects DNA binding in a dimeric *lac* repressor produced by C-terminal deletion. *Biochemistry 33*, 8728–8735.
24. Zhan, H., Swint-Kruse, L., and Matthews, K. S. (2006) Extrinsic interactions dominate helical propensity in coupled binding and folding of lactose repressor protein hinge helix. *Biochemistry 45*, 5896–5906.
25. Wong, I., and Lohman, T. M. (1993) A double-filter method for nitrocellulose-filter binding: Application to protein-nucleic acid interactions. *Proc. Natl. Acad. Sci. U.S.A. 90*, 5428–5432.
26. Falcon, C. M., and Matthews, K. S. (2001) Engineered disulfide linking the hinge regions within lactose repressor dimer increases operator affinity, decreases sequence selectivity, and alters allostery. *Biochemistry 40*, 15650–15659.
27. Laiken, S. L., Gross, C. A., and von Hippel, P. H. (1972) Equilibrium and kinetic studies of *Escherichia coli lac* repressor-inducer interactions. *J. Mol. Biol. 66*, 143–155.
28. Bourgeois, S. (1971) Techniques to assay repressors. *Methods Enzymol. 21*, 491–500.
29. Warren, J. R., and Gordon, J. A. (1966) On the refractive indices of aqueous solutions of urea. *J. Phys. Chem. 70*, 297–300.
30. Pace, C. N. (1986) Determination and analysis of urea and guanidine hydrochloride denaturation curves. *Methods Enzymol. 131*, 266–280.
31. Santoro, M. M., and Bolen, D. W. (1988) Unfolding free energy changes determined by the linear extrapolation method. 1. Unfolding of phenylmethanesulfonyl α-chymotrypsin using different denaturants. *Biochemistry 27*, 8063–8068.
32. Suckow, J., Markiewicz, P., Kleina, L. G., Miller, J., Kisters-Woike, B., and Müller-Hill, B. (1996) Genetic studies of the Lac repressor XV: 4000 single amino acid substitutions and analysis of the resulting phenotypes on the basis of the protein structure. *J. Mol. Biol. 261*, 509–523.
33. Kumar, S., and Nussinov, R. (2002) Relationship between ion pair geometries and electrostatic strengths in proteins. *Biophys. J. 83*, 1595–1612.
34. Brun, L., Isom, D. G., Velu, P., Garcia-Moreno, B., and Royer, C. A. (2006) Hydration of the folding transition state ensemble of a protein. *Biochemistry 45*, 3473–3480.
35. Derewenda, U., Swenson, L., Green, R., Wei, Y., Dodson, G. G., Yamaguchi, S., Haas, M. J., and Derewenda, Z. S. (1994) An unusual buried polar cluster in a family of fungal lipases. *Nat. Struct. Biol. 1*, 36–47.
36. Kim, J., Mao, J., and Gunner, M. R. (2005) Are acidic and basic groups in buried proteins predicted to be ionized? *J. Mol. Biol. 348*, 1283–1298.
37. Harms, M. J., Schlessman, J. L., Chimenti, M. S., Sue, G. R., Damjanovic, A., and Garcia-Moreno, B. (2008) A buried lysine that titrates with a normal pKa: Role of conformational flexibility at the protein-water interface as a determinant of pKa values. *Protein Sci. 17*, 833–845.
38. Damjanovic, A., Garcia-Moreno, B., Lattman, E. E., and Garcia, A. E. (2005) Molecular dynamics study of water penetration in staphylococcal nuclease. *Proteins 60*, 433–449.
39. Damjanovic, A., Wu, X., Garcia-Moreno, E. B., and Brooks, B. R. (2008) Backbone relaxation coupled to the ionization of internal groups in proteins: A self-guided Langevin dynamics study. *Biophys. J. 95*, 4091–4101.
40. Takano, K., Yamagata, Y., and Yutani, K. (2001) Contribution of polar groups in the interior of a protein to the conformational stability. *Biochemistry 40*, 4853–4858.
41. Waldburger, C. D., Schildbach, J. F., and Sauer, R. T. (1995) Are buried salt bridges important for protein stability and conformational specificity? *Nat. Struct. Biol. 2*, 122–128.
42. Kumar, S., and Nussinov, R. (1999) Salt bridge stability in monomeric proteins. *J. Mol. Biol. 293*, 1241–1255.
43. Yip, K. S. P., Stillman, T. J., Britton, K. L., Artymiuk, P. J., Baker, P. J., Sedelnikova, S. E., Engel, P. C., Pasquo, A., Chiaraluce, R., Consalvi, V., Scandurra, R., and Rice, D. W. (1995) The structure of *Pyrococcus furiosus* glutamate dehydrogenase reveals a key role for ion-pair networks in maintaining enzyme stability at extreme temperatures. *Structure 3*, 1147–1158.
44. Kumar, S., and Nussinov, R. (2001) How do thermophilic proteins deal with heat? *Cell. Mol. Life Sci. 58*, 1216–1233.
45. Marqusee, S., and Sauer, R. T. (1994) Contributions of a hydrogen bond/salt bridge network to the stability of secondary and tertiary structure in lambda repressor. *Protein Sci. 3*, 2217–2225.

BI801357F